ORIGINAL PAPER

The effects of metamorphism on O and Fe isotope compositions in the Biwabik Iron Formation, northern Minnesota

Elizabeth Valaas Hyslop · John W. Valley · Clark M. Johnson · Brian L. Beard

Abstract The Biwabik Iron Formation of Minnesota (1.9 Ga) underwent contact metamorphism by intrusion of the Duluth Complex (1.1 Ga). Apparent quartz–magnetite oxygen isotope temperatures decrease from $\sim 700°C$ at the contact to $\sim 375°C$ at 2.6 km distance (normal to the contact in 3D). Metamorphic pigeonite at the contact, however, indicates that peak temperatures were greater than 825°C. The apparent O isotope temperatures, therefore, reflect cooling, and not peak metamorphic conditions. Magnetite was reset in $\delta^{18}O$ as a function of grain size, indicating that isotopic exchange was controlled by diffusion of oxygen in magnetite for samples from above the grunerite isograd. Apparent quartz–magnetite O isotope temperatures are similar to calculated closure temperatures for oxygen diffusion in magnetite at a cooling rate of $\sim 5.6°C/kyr$, which suggests that the Biwabik Iron Formation cooled from ~ 825 to $400°C$ in ~ 75 kyr at the contact with the Duluth Complex. Isotopic exchange during metamorphism also occurred for Fe, where magnetite–Fe silicate fractionations decrease with increasing metamorphic grade. Correlations between quartz–magnetite O isotope fractionations and magnetite–iron silicate Fe isotope fractionations suggest that both reflect cooling, where the closure temperature for Fe was higher than for O. The net effect of metamorphism on $\delta^{18}O–\delta^{56}Fe$ variations in magnetite is a strong increase in $\delta^{18}O_{Mt}$ and a mild decrease in $\delta^{56}Fe$ with increasing metamorphic grade, relative to the isotopic compositions that are expected at the low temperatures of initial magnetite formation. If metamorphism of Iron Formations occurs in a closed system, bulk O and Fe isotope compositions may be preserved, although re-equilibration among the minerals may occur for both O and Fe isotopes.

E. V. Hyslop · J. W. Valley (✉) · C. M. Johnson · B. L. Beard
Department of Geology and Geophysics,
University of Wisconsin-Madison, 1215 West Dayton Street,
Madison, WI 53706, USA
e-mail: valley@geology.wisc.edu

Introduction

Banded Iron Formations (BIF) have played a central role in constraining surface conditions in the Precambrian Earth, including the evolution of the atmosphere (e.g., Cloud 1968). Oxygen isotope studies of BIFs have been used to estimate the temperature and isotopic compositions of Precambrian seawater (i.e., Perry and Tan 1972; Veizer and Hoefs 1976; Knauth and Lowe 2003; Perry and Lefticariu 2003). Most BIFs, however, have been metamorphosed, and oxygen isotope thermometers such as quartz–magnetite have been applied to constrain both contact and regional metamorphism (e.g., Perry and Bonnichsen 1966; Perry et al. 1973; Becker and Clayton 1976). Iron isotope data have been reported for siderite, magnetite, and hematite layers from the Kuruman and Griquatown iron formations from the Transvaal Craton, South Africa, which have been only weakly metamorphosed ($\sim 110–170°C$) (Johnson et al. 2003), and Fe isotope compositions for magnetite have been interpreted to reflect mixtures between mid-ocean ridge hydrothermal and bacterial sources (Johnson et al. 2005). Dauphas et al. (2004, 2007) reported Fe isotope data for

Fig. 1 Geologic map and cross section of the Biwabik Iron Formation and surrounding formations, with average dip of the contact with the Duluth Complex. The cross section shows stratigraphic relations. The numbered contours in the Duluth Complex represent depth (m) to the contact with the country rock. Modified from Bonnichsen (1972)
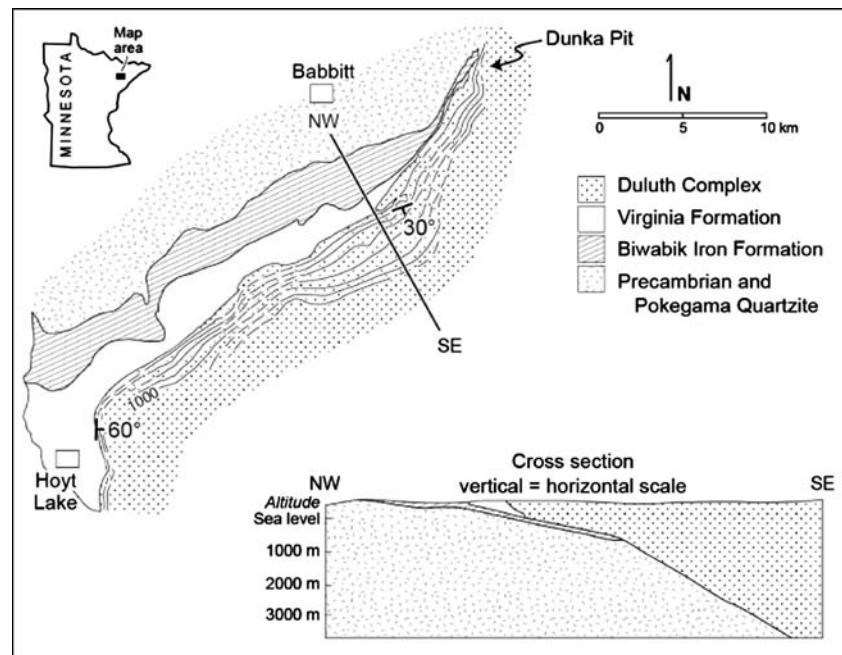
high-grade (up to granulite facies) banded rocks from SW Greenland and Canada, and interpreted these to record primary sedimentary compositions. Frost et al. (2007) conducted the first Fe isotope study of the effects of contact metamorphism of the Biwabik Iron Formation, and they conclude that the isotopic compositions of magnetite were not changed during metamorphism relative to their pre-metamorphic compositions.

This study presents O and Fe isotope compositions of the eastern exposures of the Biwabik Iron Formation (northern Minnesota) that were contact metamorphosed by the Duluth Complex (Valaas 2004). In the Biwabik Iron Formation, previous studies have used quartz–magnetite O isotope temperatures to study thermal gradients during contact metamorphism (e.g., Perry and Bonnichsen 1966). However, metamorphic pigeonite (2–7% $MnSiO_3$; Bonnichsen 1969), and the orthopyroxene-pigeonite phase boundary indicate a minimum temperature of 825°C at the contact (Lindsley 1983), which is over 100°C above the quartz–magnetite O isotope temperatures of Perry and Bonnichsen (1966), suggesting that this thermometer has been reset. This study examines the question of whether such temperatures are representative of peak metamorphic conditions (thermometry) or post metamorphic cooling rates (speedometry) in the Biwabik Iron Formation. In addition, Fe isotope compositions were measured in the Biwabik rocks to investigate the effects of metamorphism with proximity to the contact with the Duluth Complex; our work expands on that reported in Frost et al. (2007), comes to different conclusions regarding Fe isotope thermometry, and evaluates the viability of the chemical leaching methods they employed. The goal of the present study is to

deepen our understanding of O and Fe isotope behavior during metamorphism of BIFs, given the fact that most Archean BIFs have been metamorphosed to amphibolite- to granulite-grade.

Regional geology

The Mesabi iron range is a 0.5–5 km wide package of rocks that strikes for 190 km from southwest to the northeast in northern Minnesota, where it is truncated by the Duluth Complex near Babbitt, Minnesota (Fig. 1) (Perry and Bonnichsen 1966; Morey 1983; Ojakangas et al. 2005). Collectively the Mesabi iron range rocks are part of the Animikie Group, which are correlative with rocks from the Gunflint and Cuyuna Iron Ranges of Ontario and Minnesota (e.g., Morey and van Schmus 1988). The Animikie Group sedimentary rocks, as well as similar rocks to the southeast which include the Gogebic, Marquette, and Menominee iron ranges of Michigan and Wisconsin were deposited in the Animikie Basin (e.g., Morey and van Schmus 1988).

Deposition of the Biwabik Iron Formation occurred prior to 1,850 Ma as constrained by a U–Pb analysis on zircon from an ash layer that occurs in the lower part of the Virginia Formation, which is stratigraphically above the Biwabik Iron Formation (Hemming et al. 1996). Additionally, near concordant U–Pb analyses of euhedral zircons that occur in a volcaniclastic layer within the Gunflint Iron Formation, which is correlative with the Biwabik Iron Formation, indicate a deposition age of 1,878 ± 1.3 Ma (Fralick et al. 2002). The Biwabik and
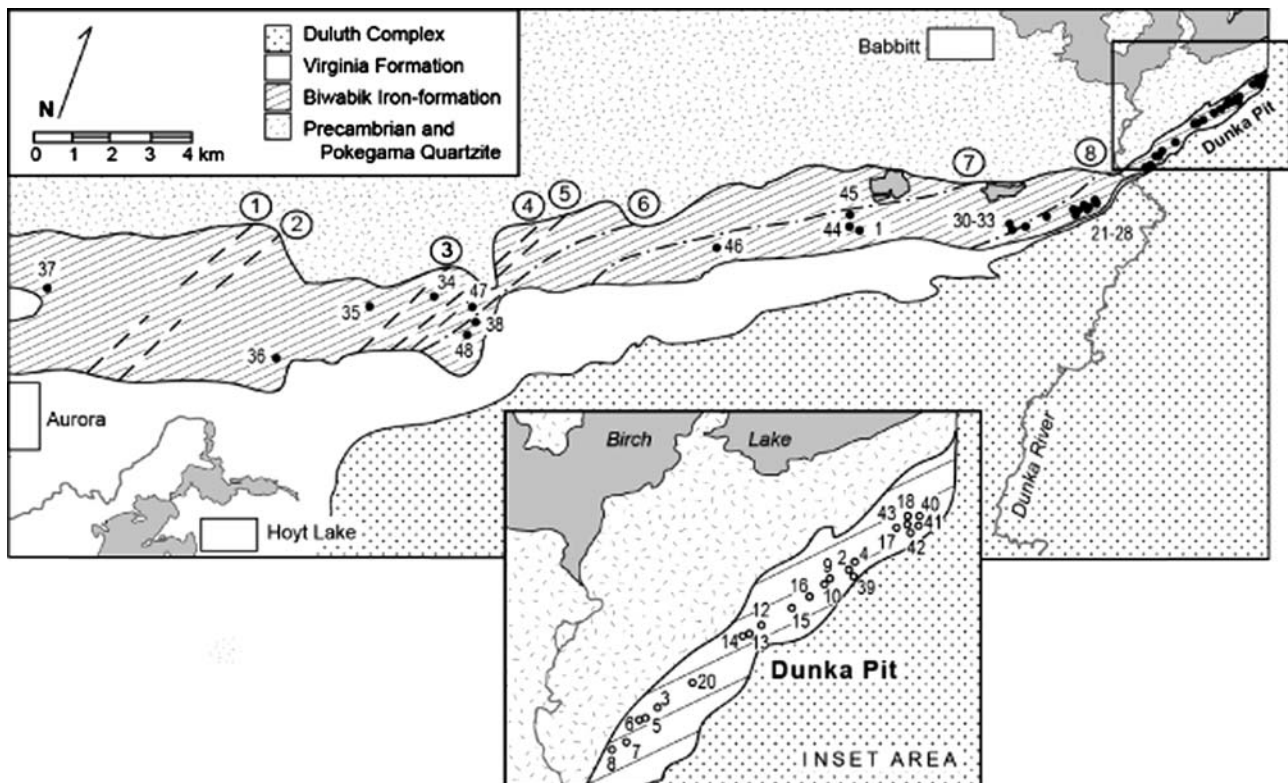
Fig. 2 Map showing isograds (*numbers in circles*) and sample locations (*dots*) from the Upper Cherty member of the Biwabik Iron Formation. The isograds of French (1968) (*dashed lines*) are as follows: (*1*) partial reduction of hematite to magnetite; (*2*) formation of clinozoisite; (*3*) formation of grunerite; (*4*) formation of heden-bergite and complete reduction of hematite to magnetite (note that two close isograds were condensed to one for the scale of this map); (*5*) formation of ferrohypersthene coupled with graphite. The isograds of Frost et al. (2007) (*dash-dot-dash lines*) are also shown: (*3*) amphibole (equivalent to isograd 3 of French 1968); (*6*) hedenbergite; (*7*) fayalite; (*8*) orthopyroxene. Metamorphic reactions are summarized in Table 1

Gunflint Iron Formations are along strike with each other and were likely a continuous formation that is now separated by intrusion of the Duluth Complex. Four stratigraphic divisions are recognized in the Biwabik Iron Formation, the Lower Cherty, Lower Slaty, Upper Cherty, and Upper Slaty (Gundersen and Schwartz 1962; Bon-nichsen 1975; Morey 1992; Ojakangas et al. 2005). The cherty layers are massive, richer in quartz and magnetite, and have a more granular texture where not highly meta-morphosed, suggesting that the layers were deposited in shallow water, high-energy environment. In contrast, the slaty layers are fine grained, laminated, rich in iron silicates and carbonates, relatively magnetite-poor, and were deposited in a deeper water, low-energy environment.

Sedimentary bedding dips 45°–30° southeast in the northeast part of the study area (Fig. 1), closest to the contact with the Duluth Complex, and shallows to 5° within a few km along strike to the southwest. The contact between the Duluth Complex and the iron formation country rock dips 20°–30° SE along the northwestern edge of the intrusion (the northeastern portion of Fig. 1), and systematically increases to as much as 60°E (Fig. 1).

Emplacement of the Duluth Complex (1,106–1,096 Ma; Hauck et al. 1997), contemporaneous with Keweenawan rifting, resulted in contact metamorphism of the Biwabik Iron Formation (Weiblen and Morey 1980; Hauck et al. 1997). The Duluth Complex is composed of a variety of rock types, including troctolite, gabbro, anorthosite, granodiorite, and granite. The Biwabik Iron Formation was intruded by the troctolitic South Kawishiwi and Partridge River intrusions (Weiblen and Morey 1980; Hauck et al. 1997). Emplacement temperature of the Duluth Complex is estimated at ∼1,150°C based on phase equilibria and an inferred local parent magma: 32% ferrodioritic liquid plus 68% suspended crystals of plagioclase and olivine (Cha-lokwu et al. 1993; Koptev-Dornikov et al. 1995). Pyroxene hornfels-facies metamorphism in the Biwabik Iron For-mation occurs nearest to the contact (Hauck et al. 1997).

Isograds have been mapped in the Biwabik Iron For-mation and are sub-parallel to the present contact with the Duluth Complex (French 1968). The eight isograds shown in Fig. 2 are defined by: (1) partial reduction of hematite to magnetite, (2) clinozoisite, (3) grunerite, (4) hedenbergite and the complete reduction of hematite to magnetite, and

Table 1 List of metamorphic reactions in the Biwabik Iron Formation

Mineral	Reaction
Minnesotaite	Greenalite + 2 quartz = minnesotaite + water[a]
	$(Fe,Mg)_3Si_2O_5(OH)_4 + 2SiO_2 = (Fe,Mg)_3Si_4O_{10}(OH)_2 + H_2O$
	3 Siderite + 4 quartz + H_2O = minnesotaite + $3CO_2$[a]
	$3(Fe,Mg)CO_3 + 4SiO_2 + H_2O = (Fe,Mg)_3Si_4O_{10}(OH)_2 + 3CO_2$
Grunerite	7 Minnesotaite = 3 grunerite + 4 quartz + $4H_2O$[a]
	$7(Fe,Mg)_3Si_4O_{10}(OH)_2 = 3(Fe,Mg)_7Si_8O_{22}(OH)_2 + 4SiO_2 + 4H_2O$
Hedenbergite	Ankerite + 2 quartz = hedenbergite + $2CO_2$[b]
	$CaFe(CO_3)_2 + 2SiO_2 = CaFeSi_2O_6 + 2CO_2$
Fayalite	2 Grunerite = 7 fayalite + 9 quartz + $2H_2O$[b]
	$2(Fe,Mg)_7Si_8O_{22}(OH)_2 = 7(Fe,Mg)_2SiO_4 + 9SiO_2 + 2H_2O$
	2 Magnetite + 3 quartz = 3 fayalite + O_2[b]
	$2Fe_3O_4 + 3SiO_2 = 3Fe_2SiO_4 + O_2$
	2 Siderite$_{ss}$ + quartz = fayalite$_{ss}$ + $2CO_2$[b]
	$2(Fe,Mg)CO_3 + SiO_2 = (Fe,Mg)_2SiO_4 + 2CO_2$
Orthopyroxene	Olivine + quartz = 2 orthopyroxene[a]
	$(Fe,Mg)_2SiO_4 + SiO_2 = 2(Fe,Mg)SiO_3$
	Grunerite + siderite = 8 orthopyroxene + CO_2 + H_2O[c]
	$(Fe,Mg)_7Si_8O_{22}(OH)_2 + (Fe,Mg)CO_3 = 8(Fe,Mg)SiO_3 + CO_2 + H_2O$

[a] Bonnichsen (1975)
[b] French (1968)
[c] Miyano and Klein (1986)

(5) ferrohypersthene along with the development of crystalline graphite. These isograds have been refined and expanded by Frost et al. (2007) to include formation of: (6) hedenbergite, (7) fayalite, and (8) orthopyroxene.

Rock and sample descriptions

Sampling localities are shown in Fig. 2 (see also Valaas 2004). Distances to the contact listed in the tables are estimated in three dimensions (3D) normal to the contact. The 3D distances are projected perpendicular to the basal contact of the Duluth Complex. For simplicity, a dip of 30° was assumed for the northern part, and 60° for samples in the southwestern part of the study area.

Grain sizes regularly increase toward the contact with the Duluth Complex due to metamorphic re-crystallization (Table S1; On-Line Supplementary Material), but sedimentary features are preserved at distances greater than 3 km from the contact. All samples are from the Upper Cherty unit of the Biwabik Iron Formation. This unit was chosen due to its excellent exposures in mine workings and for its high magnetite content, which averages 26% by mode. Mineral modes, as determined using digital image analysis, are given in Table S1.

Changes in mineralogy toward the contact with the Duluth Complex affect the O and Fe repositories, which in turn may affect their isotopic compositions. We have confirmed previously mapped isograds (Fig. 2; French 1968; Frost et al. 2007) through thin section examination. In addition to quartz (originally chert) + magnetite, the

samples furthest from the contact may contain siderite, ankerite, greenalite, minnesotaite, or stilpnomelane. At 2–3 km from the contact, the assemblage is quartz + magnetite + grunerite ± carbonate. Closer to the contact, the assemblage shifts to quartz + magnetite ± grunerite ± cummingtonite ± actinolite ± hedenbergite ± fayalite. Inverted pigeonite is recognized by reintegration of exsolution lamellae in the host orthopyroxene. Orthopyroxene appears closest to the contact. The reactions that form the metamorphic minerals in the Biwabik rocks are given in Table 1. Actinolite, where present, typically rims grunerite or cummingtonite. Cummingtonite and actinolite from nearer the contact were likely formed by retrograde reactions involving fayalite and pyroxene breakdown (Bonnichsen 1975).

In samples less than 50 m from the contact, quartz and magnetite occur as coarse grains (>400 μm average diameter), and quartz layers are thicker (∼20–100 mm) than magnetite layers (∼2–8 mm). Petrographic relations indicate complete metamorphic re-crystallization and growth of new magnetite and pyroxene. Samples from 100 to 3,000 m distance (estimated in 3D) show a gradational shift to finer grain sizes with increasing distance (Table S1), and quartz layers are ∼20–100 mm and magnetite layers are ∼1–5 mm in thickness in this interval. Quartz and magnetite oolitic and non-oolitic granules locally persist in quartz layers at 100–2,600 m distance. Samples that are over 2,600 m from the contact are more fine grained and consistently preserve sedimentary granules and oolitic and non-oolitic shapes in a quartz (chert) matrix.

Methods and nomenclature

Sample preparation

Each sample is identified in the tables by the following numbering system: 03 BIW XYZ, where X = outcrop number, Y = letter to differentiate hand samples collected 0.1–10 m apart, Z = number that differentiates areas of interest in a hand sample (if necessary). Samples followed by M1, 2, or 3 indicate individual magnetite layers analyzed in a single ~800 μm thick microscope slide. No samples were collected from 170 to 1,250 m distance from the contact due to active mining or mine flooding.

Quartz and magnetite were hand-picked for analysis from coarse samples (mineral grains of ~150–1,000 μm diameter) located closer to the contact (Dunka Pit, 0–33 m, 3D). Grains greater than ~150 μm in diameter were separated by hand magnet to concentrate the magnetite from the quartz and other silicates. The magnetite concentrate was not acid treated, but picked directly for both oxygen and iron isotope analysis. Quartz and Fe-silicate mineral separates were treated in 12 M HCl at room temperature for 2–3 h to remove any residual magnetite, and then further purified by hand picking. Quartz and Fe silicates showed no sign of attack by this treatment, and solutions were clear to pale yellow, indicating that some samples contained no magnetite, nor was pyroxene dissolved. Quantitative partial dissolution tests (below) confirmed negligible dissolution of Fe silicates by the 12 M HCl treatment.

Samples that were greater than 100 m from the contact (3D) were processed differently due to the finer grain size. Quartz and Fe-silicates were hand picked after HCl treatment. For magnetite, thick sections (0.8 mm thick) were cut with a thin diamond saw blade along magnetite-rich layers, which produced strips ~0.8 × 1 × 20 mm; the dimensions depended on the layer of interest. Pieces weighing approximately 2 mg (~0.5 mm^3) were selected from the strips of magnetite-rich layers for O isotope analysis. Adjacent material, on strike, was set aside to test purity of magnetite and for iron isotope analysis. The amount of silicate impurities in these magnetite samples is important to assess for O isotope analyses, and was estimated from the weight change upon dissolution of magnetite in HCl. Samples that contained greater than 20 wt% silicates were rejected for O isotope analysis. Magnetite samples with 0–20% of silicates were corrected for oxygen isotope compositions as described below. Because most of the silicate contamination in the magnetite separates consisted of quartz, the Fe isotope analyses of magnetite are not affected by silicate impurities. Due to the fine-grained nature of the Fe silicate minerals, it was not possible to obtain separates of distinct minerals for Fe isotope analysis, and the "Fe silicate" aliquot contains a mixture of minerals as noted in the associated tables.

Partial dissolution tests

The effectiveness of partial dissolution of the BIFs to isolate carbonate, oxide, or silicate components for Fe isotope analysis, an approach used by Frost et al. (2007) in their study of the Biwabik Iron Formation, was evaluated using pure siderite and magnetite powders and 0.75 and 1.0 M HCl, as well as 20% acetic acid (HAc) treatment over variable time and temperature. The efficiency of HCl and HAc treatment in dissolving pure siderite powder was determined in anticipation that this might be the first treatment of powdered rock samples, and parallel experiments were done on pure magnetite powder to determine any contributions of magnetite in partial dissolution of a magnetite–siderite mixture. Fe(II) and total Fe (Fe$_{Total}$) contents in the magnetite dissolution tests were determined using the *Ferrozine* method (Stookey 1970) to determine if partial magnetite dissolution occurs congruently, followed by Fe isotope analysis of the supernatant and residue. In addition, sized mineral separates of orthopyroxenes obtained from magnetite-free museum specimens were subjected to 0.5 and 12 M HCl treatment to determine the extent of silicate dissolution in samples that were analyzed for Fe isotope compositions.

Oxygen isotope analysis

Oxygen was extracted from 0.5 to 1.5 mg of quartz and 1.7–2.8 mg of magnetite by laser heating and fluorination with BrF$_5$ as the reagent (Valley et al. 1995; Spicuzza et al. 1998). The liberated oxygen was converted to CO$_2$ for analysis on a Finnigan MAT 251 mass spectrometer at the University of Wisconsin-Madison. Oxygen isotope ratios are reported using standard delta (δ) notation in units of per mil (‰), relative to V-SMOW. An internal standard, UWG-2 (Gore Mountain garnet), was run ~6 times on each day of analysis. The variation in $\delta^{18}O$ values for UWG-2 yielded a mean daily standard deviation of ±0.08‰ (1SD). All data were corrected to a $\delta^{18}O$ value for UWG-2 of +5.80‰ (Valley et al. 1995) for accuracy; the average correction was 0.11‰. Four analyses of NBS-28 (quartz) yielded $\delta^{18}O$ = +9.50 ±0.06‰, when normalized to UWG-2.

Iron isotope analysis

Powdered samples were completely digested in heated Teflon beakers using concentrated HF and HNO$_3$. Iron was separated from the bulk sample using anion-exchange chromatography and anion exchange resin (Bio-Rad AG 1 × 4 200–400 mesh). Iron contents of the separated solution were determined using the *Ferrozine* method (Stookey

1970), which allowed Fe concentrations for MC-ICP-MS analysis to be matched to those of standards and to check that ion-exchange column yields were 100%. Iron isotope analyses were made by MC-ICP-MS (Micromass *IsoProbe*) equipped with a collision cell and a micro-concentric desolvating nebulizer (Cetac *Aridus*) at the University of Wisconsin-Madison. A standard-sample-standard bracketing method was used to correct for instrumental mass bias, which produces accurate results if the separated Fe solutions are pure, such that the sample matrix matches that of the standards (Albaréde and Beard 2004).

Iron isotope compositions are reported using standard delta (δ) notation in per mil (‰) relative to the average of igneous rocks (Beard et al. 2003): $\delta^{56}Fe = [(^{56}Fe/^{54}Fe)_{sample}/(^{56}Fe/^{54}Fe)_{Ig\ Rxs} - 1] \times 10^3$. Values of $\delta^{57}Fe$ are defined in an analogous manner using $^{57}Fe/^{54}Fe$ ratios. Comparison between laboratories may be made through the IRMM-14 Fe standard, which has a $\delta^{56}Fe$ value of -0.09 ± 0.05‰ (Beard et al. 2003) on the igneous rock scale. External reproducibility in $\delta^{56}Fe$ values is ±0.05‰ based on the precision of three standards that were run during the time period in which samples were measured: UW J-M Fe: $\delta^{56}Fe = +0.25 \pm 0.05$‰, $\delta^{57}Fe = +0.39 \pm 0.07$‰ ($n = 47$); UW HPS Fe: $\delta^{56}Fe = +0.49 \pm 0.05$‰, $\delta^{57}Fe = +0.74 \pm 0.07$‰ ($n = 52$); IRMM-14 Fe: $\delta^{56}Fe = -0.09 \pm 0.05$‰, $\delta^{57}Fe = -0.11 \pm 0.07$‰ ($n = 54$), where all uncertainties are 1σ (SD) external standard deviations. Ten samples were duplicated or triplicated through mass analysis of the same solution on different days, which produced an average 1σ SD of ±0.03‰, suggesting that the average external 2σ reproducibility for these samples is ±0.06‰. Three samples were duplicated through dissolution and chemical separation of different aliquots of the solid sample, and the 1σ SD of the aliquots ranged from ±0.01 to ±0.13‰; some of this variability may reflect small isotopic heterogeneity in the samples.

Isotopic fractionations

Apparent temperatures of the Biwabik Iron Formation are calculated using the well-calibrated quartz–magnetite oxygen isotope thermometer. We define the quartz–magnetite fractionation factor as:

$$\Delta^{18}O_{Qtz-Mt} = \delta^{18}O_{Qtz} - \delta^{18}O_{Mt} \approx 10^3 \ln \alpha^{18}O_{Qtz-Mt} \quad (1)$$

where $\alpha^{18}O_{Qtz-Mt}$ is the quartz–magnetite $^{18}O/^{16}O$ fractionation factor. Using the calibration of Clayton and Kieffer (1991),

$$10^3 \ln \alpha^{18}O_{Qtz-Mt} = 6.29 \times 10^6/T^2 \quad (2)$$

where T is in K. The O isotope compositions of magnetite have been corrected for minor silicate impurities, as

discussed in Appendix 1 and listed in Table S2 of the On-Line Supplementary Material; whole-rock $\delta^{18}O$ values ($\delta^{18}O_{WR}$) have been calculated using the methods outlined in Appendix 2 and listed in Table S3:

$$\delta^{18}O_{WR} = X_{Qtz} \times \delta^{18}O_{Qtz} + X_{Mt} \times \delta^{18}O_{Mt} \quad (3)$$

where X_{Qtz} and X_{Mt} are the O molar fractions of quartz and magnetite, respectively. The modal amounts of quartz and magnetite, as determined using digital image analysis of thin sections, are from Table S1. Minerals other than magnetite were estimated as quartz. The amount of silicates other than quartz varied (5–65%), but the mode % of quartz generally decreased with increasing metamorphic grade. Estimates of $\delta^{18}O_{WR}$ are therefore most reliable for the least metamorphosed, quartz-rich samples.

We define the magnetite–Fe silicate fractionation factor as:

$$\Delta^{56}Fe_{Mt-Fe\ Sil} = \delta^{56}Fe_{Mt} - \delta^{56}Fe_{Fe\ Sil} \approx 10^3 \ln \alpha^{56}Fe_{Mt-Fe\ Sil} \quad (4)$$

where $\alpha^{56}Fe_{Mt-Fe\ Sil}$ is the magnetite–Fe silicate $^{56}Fe/^{54}Fe$ fractionation factor. Because of the mixed nature of the Fe silicate mineral separates, we compare our results to two thermometers, magnetite–olivine and magnetite–hedenbergite:

$$10^3 \ln \alpha^{56}Fe_{Mt-Ol} = 0.270 \times 10^6/T^2 \quad (5)$$

and

$$10^3 \ln \alpha^{56}Fe_{Mt-Hed} = 0.335 \times 10^6/T^2 \quad (6)$$

where T is in K, using the predicted Fe isotope fractionation factors from Polyakov and Mineev (2000) and Polyakov et al. (2007). Values of $\delta^{56}Fe$ for magnetite and Fe silicates are taken as measured from the mineral separates. Whole-rock $\delta^{56}Fe$ values are calculated in a manner similar to that used for $\delta^{18}O_{WR}$ calculations (Appendix 2), and are given in Table S4.

Pyroxene analysis

Pyroxene compositions were determined by wavelength-dispersive spectroscopy (WDS) on the CAMECA SX51 electron microprobe at the University of Wisconsin-Madison. The electron microprobe was operated at 15 keV with 20 nA of Faraday cup current in fixed spot mode with a focused beam. Standards were natural and synthetic olivines and pyroxenes and synthetic TiO_2. For inverted pigeonite, compositions of host and lamellae were reintegrated to determine the original pigeonite composition using digital image analysis to estimate volumes of lamellae and host from BSE images.

Results

The chemical compositions of pyroxenes were determined in five samples (Table S5). Oxygen isotope compositions were determined on quartz and magnetite for 63 samples of the Biwabik Iron Formation from the contact with the Duluth Complex to 2,728 m away (3D distance; Table S6). The results of partial dissolution tests for Fe isotope analysis are given in Table S7. Magnetite from 27 samples was analyzed for Fe isotope compositions, and co-existing Fe silicates were analyzed in 11 of these samples (Table S8).

Pyroxene compositions and temperatures

Bonnichsen (1969) reported non-exsolved and inverted metamorphic pigeonite close to the contact with the Duluth Complex, and our observations support this. We analyzed pyroxenes between 0 and 33 m distance from the contact (Table S5) and found inverted pigeonite at distances up to 8 m (Fig. 3). The inverted pigeonite occurs in the coarsest BIF at Dunka Pit. The least Mn-rich pigeonite contains 2.0 mol% Mn. This value is important because it provides the most restrictive estimate of minimum temperature of metamorphism at the contact. The reintegrated pigeonite compositions (Table S5) suggest a minimum temperature at the contact of ≥825°C (Lindsley 1983). Simmons et al. (1974) estimated the temperature at the contact of the Duluth Complex and the Gunflint Iron Formation to be >825°C at a locality 60 km NE using two pyroxene thermometry (pigeonite and augite), which agrees well with our estimate.

Anomalous Fe isotope fractionation upon incongruent partial dissolution of samples

The complex mineralogy and fine-grained nature of many Biwabik samples led Frost et al. (2007) to attempt determination of Fe isotope compositions of carbonate, oxide,
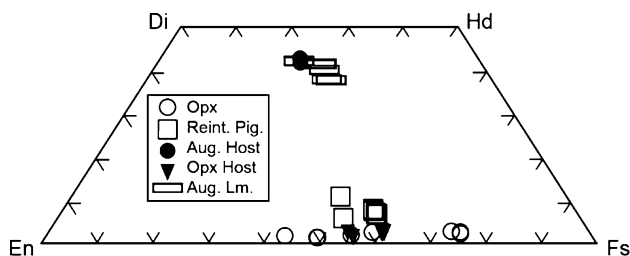

Fig. 3 Compositions of augite, orthopyroxene, and re-integrated pigeonite. The *triangles* and *rectangles* represent the host and lamellae of inverted pigeonite, *circles* are measured pyroxenes and *squares* are re-integrated pigeonites. Data from Table S5

and silicate components through magnetic separation and HAc, HCl, and HF partial dissolution. The supernatants were analyzed by ICP-AES to monitor the phases dissolved, although such analysis cannot, for example, detect partial dissolution of magnetite in the carbonate fractions that were determined by HAc treatment. Frost et al. (2007) attempted to isolate the majority of magnetite through an initial magnetic separation, although they document residual magnetite in the "non-magnetic" fractions that were treated with HAc to dissolve carbonate.

We found that complete dissolution of siderite powder required more aggressive HAc treatment (20% HAc, 40°C, >24 h; Table S7) than that used by Frost et al. (2007) (10% HAc at room temperature), although the less aggressive treatment would likely dissolve dolomite and calcite. More importantly, however, was the observation that HAc treatment incongruently dissolves magnetite where the solution has $Fe(II)/Fe_{Total}$ ratios higher than 0.33. These solutions had anomalously low-$\delta^{56}Fe$ values by ∼0.4‰ in the supernatant relative to the initial magnetite composition (Table S7). These results indicate that HAc treatment of carbonate–magnetite mixtures may produce anomalous Fe isotope compositions that do not reflect either the carbonate or the magnetite components; the effects are likely to be most significant where the carbonate is dolomite or calcite, which have much lower Fe contents than siderite. In contrast, HCl treatment congruently dissolves magnetite, as indicated by the stoichiometric $Fe(II)/Fe_{Total}$ ratios and $\delta^{56}Fe$ values that are identical to the initial magnetite composition (Table S7). These results are similar to HCl dissolution of hematite, which occurs congruently and imparts no anomalous Fe isotope compositions (Johnson et al. 2004). Nevertheless, given the broad overlap in the extent of dissolution of magnetite and siderite in HCl under similar conditions, we did not attempt to partially dissolve the carbonate component in the samples.

Finally, we determined the extent of dissolution of pure orthopyroxene mineral separates in 0.5 and 12 M HCl (Table S7) to test that validity of our HCl treatment of the Fe silicate component that is intended to remove trace quantities of magnetite. Long-term (up to 96 h) treatment in warm 0.5 M HCl dissolved only 1.9% of the orthopyroxene, but such treatment would not significantly dissolve magnetite contaminants. Treatment in 12 M HCl at room temperature for 2–3 h completely dissolves magnetite, and produces only 0.4–2.0% dissolution of the orthopyroxene, where the largest extent of dissolution occurred in the fine-grained samples; for the relatively coarse-grained Fe silicate mineral separates analyzed in this study, these tests show that the 12 M HCl treatment can have no effect on the Fe isotope compositions that were determined.
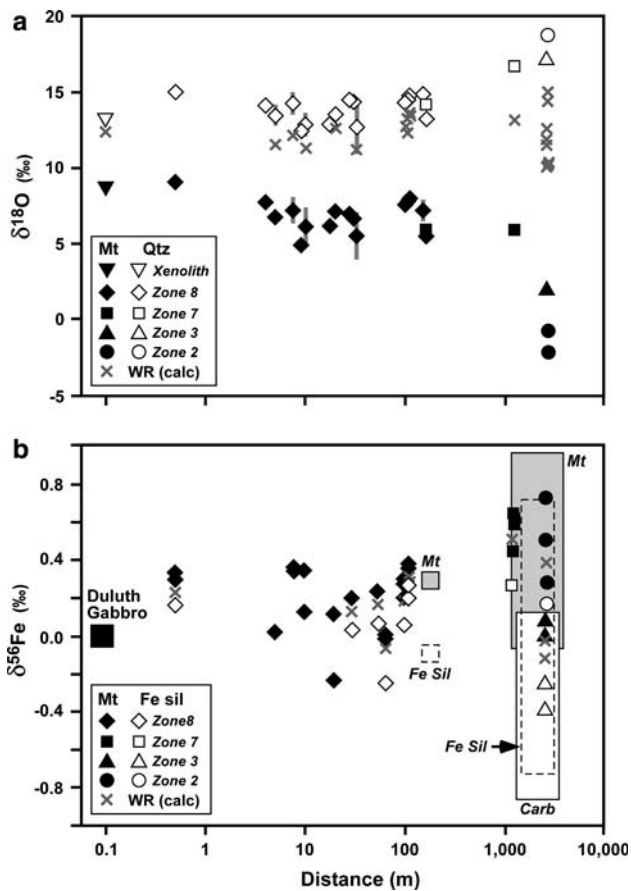
Fig. 4 Oxygen and Fe isotope variations with 3D distance from the contact with the Duluth Complex. **a** $\delta^{18}O_{Qtz}$, $\delta^{18}O_{Mt}$, and $\delta^{18}O_{WR}$ values. Values of $\delta^{18}O_{WR}$ are calculated from modal abundances (see text). *Vertical bars* indicate uncertainty as calculated from 1σ standard deviation of isotopic compositions determined on *thick sections*. Analytical uncertainty is less than the size of the *symbols*. In all cases $\delta^{18}O_{Qtz} > \delta^{18}O_{Mt}$. Note that the change in $\delta^{18}O_{Qtz}$ values is less than that of the $\delta^{18}O_{Mt}$ values, reflecting the relatively high quartz modal abundances. Data from Tables S3 and S6. **b** $\delta^{56}Fe_{Mt}$, $\delta^{56}Fe_{Fe\ Sil}$, and $\delta^{56}Fe_{WR}$ values. $\delta^{56}Fe_{WR}$ values are calculated from modal abundances (see text). In all cases, $\delta^{56}Fe_{Mt} > \delta^{56}Fe_{Fe\ Sil}$. Data from Tables S4 and S8, and *boxes* are from Frost et al. (2007)

O and Fe isotope variations with distance

The variations in isotopic composition with distance to the contact with the Duluth Complex are distinct for O and Fe. Values of $\delta^{18}O$ for quartz and magnetite systematically decrease and increase, respectively, with proximity to the contact (Fig. 4a). The largest change in $\delta^{18}O$ values occur for magnetite, which is consistent with modal abundances. The Biwabik rocks have a greater proportion of oxygen in silicates than magnetite, where the average mode is generally 74% silicates and 26% magnetite, and the quartz/magnetite molar oxygen ratio is 1.9. If isotopic re-equilibration occurred during metamorphism, a greater shift in $\delta^{18}O_{Mt}$ would occur if isotopic exchange took place in a closed system, based on mass balance constraints (Gregory

et al. 1989). In contrast, $\delta^{56}Fe_{Mt}$ and $\delta^{56}Fe_{Fe\ Sil}$ values do not systematically change with proximity to the contact (Fig. 4b). In all cases $\delta^{56}Fe_{Mt}$ values are greater than $\delta^{56}Fe_{Fe\ Sil}$ values, and this difference is largest further from the contact. There are, however, no systematic changes in the average $\delta^{56}Fe_{Mt}$ or $\delta^{56}Fe_{Fe\ Sil}$ values for the four isograd zones that were analyzed. The general lack of correlation between $\delta^{56}Fe$ values in part reflects the wide range in magnetite and Fe silicate modes. For example, the mol% Fe that resides in magnetite ranges from 40 to 90%, but is not correlated with $\delta^{56}Fe_{Mt}$ values (Tables S1, S8).

The five localities studied by Frost et al. (2007) lie at >100 m distance (3D) from the contact, and the $\delta^{56}Fe$ values they measured for magnetite, or inferred for Fe silicates based on HF partial dissolutions, broadly overlap the range for these minerals we measure at these distances (Fig. 4). Frost et al. (2007) additionally report Fe isotope compositions for carbonates, as inferred from HAc extractions, and these extend to the most negative values measured for the Biwabik Iron Formation (Fig. 4). Although low-$\delta^{56}Fe$ values are expected for BIF carbonates (Johnson et al. 2003), the values measured by Frost et al. (2007) might also reflect, at least in part, incongruent dissolution of residual oxides in the HAc extractions, based on the partial dissolution tests above.

Discussion

The changes in O isotope compositions with distance from the contact with the Duluth Complex reflect the effects of isotopic equilibration during metamorphism followed in some cases by retrograde exchange. The degree of O isotope exchange on the hand sample and outcrop scale is discussed, followed by a discussion on Fe isotope equilibration between magnetite and Fe silicate. Finally, we discuss how premetamorphic O and Fe isotope compositions might be inferred if the effects of metamorphism are understood.

Apparent quartz–magnetite oxygen isotope temperatures

The systematic decrease in $\Delta^{18}O_{Qtz\text{-}Mt}$ fractionations with proximity to the contact may be interpreted to reflect increasing metamorphic temperatures (Figs. 5, 6). At the *mm-scale* for mineral separates or chips cut from the same thick sections (Table S6), the average 1σ standard deviation (SD) for samples closer than 2.6 km to the contact is 0.07‰ for quartz, which lies within analytical error. The average 1σ SD is 0.10‰ for magnetite, which is just outside analytical error, although one sample (31C) has a larger 1σ SD
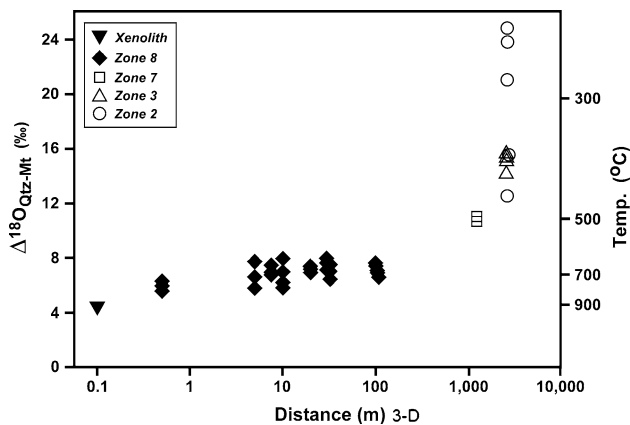
Fig. 5 Variations in quartz–magnetite O isotope fractionations ($\Delta^{18}O_{Qtz-Mt}$) with distance from the contact (3D) with the Duluth Complex. Only data from outcrops that have at least three hand samples are plotted. Corresponding temperatures (Eq. 2) shown at right. Data from Table S6

of 0.82‰. With this one exception, these results could suggest that O isotope equilibration was attained for most samples at the mm-scale. However, these data do not preclude retrograde exchange at a smaller scale.

To evaluate the degree of O isotope equilibrium at a larger scale, multiple hand samples were analyzed from 13 locations, where the size of the outcrop ranges from 2 to 10 m in length. In Fig. 5, we have plotted isotopic fractionations from all outcrops that contain three or more analyzed hand samples. The variability in $\Delta^{18}O_{Qtz-Mt}$ fractionations between hand samples in an outcrop is greater than the variability that is found within hand samples. The variability in $\Delta^{18}O_{Qtz-Mt}$ fractionations increases dramatically at greater than 2.6 km from the contact with the Duluth Complex (zone 2, outcrop 35; Fig. 5) showing that quartz and magnetite never attained isotopic equilibrium at the hand sample scale (10 cm) in outcrop 35 (zone 2), which has been excluded from further consideration in this study.

Comparison of the apparent quartz–magnetite O isotope temperatures with those predicted by pigeonite stability or simple cooling models suggests that the O isotope temperatures were reset during cooling (Fig. 6). The average apparent O isotope temperature closest to the contact is 700°C (as calculated from a polynomial curve fit; Fig. 6). The only significant deviation from this curve is sample 03 BIW 39C, which is an iron-formation xenolith within the Duluth Complex that yields 918 ± 6°C (Fig. 6). Apparent temperatures decrease from ∼700°C at the contact to ∼370°C at 2,600 m (Fig. 6). The data of Perry and Bonnichsen (1966) are also plotted in Fig. 6 with their estimates of distance in 3D, which assumes a dip of ∼12° (Perry et al. 1973). The apparent temperatures of Perry and Bonnichsen (1966), recalculated using Eq. 2, are ∼50°C lower than those we determined closest to the contact,
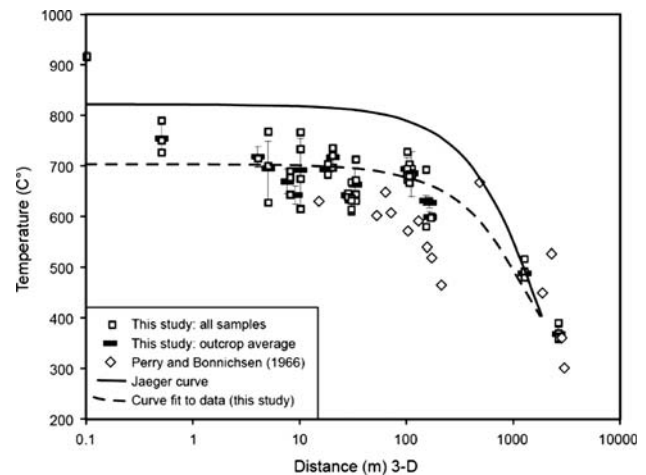

Fig. 6 Comparison of apparent quartz–magnetite O isotope temperatures from this study and Perry and Bonnichsen (1966) with distance (3D) from the contact with the Duluth Complex (Table S11). The uncertainty in the temperature is based on the 1σ standard deviation of the $\Delta^{18}O_{Qtz-Mt}$ fractionations determined from the hand samples for each outcrop. Perry and Bonnichsen's (1966) samples are generally lower in temperature than this study. The solid curve is a predicted thermal profile (Jaeger 1959) (see text). The dashed curve is a second-order polynomial fit through the data and is concave up (vs. linear T), which is consistent with conductive cooling of a simple tabular intrusive body (Jaeger 1957)

and ∼50°C higher than our result at greater than 400 m from the contact (Fig. 6, Table S11). The pigeonite temperature of >825°C that we obtain is more than 100°C above the quartz–magnetite O isotope temperature we determine at the contact and >150°C above the recalculated apparent temperature of Perry and Bonnichsen (1966).

A simple conductive cooling model is illustrated in Fig. 6, following the approach of Jaeger (1957). Details of the calculation are given in Appendix 3 (On-Line Supplementary Material). At distances less than 1,000 m, the predicted thermal profile for the Biwabik Iron Formation is higher in temperature than the curve fit through the apparent temperatures that are calculated from the measured $\Delta^{18}O_{Qtz-Mt}$ fractionations, and the greatest discrepancy exists close to the contact (Fig. 6). We therefore interpret the difference between the predicted and oxygen isotope temperature profiles to record retrograde exchange at all but the lowest temperatures; as noted above, the wide range in $\Delta^{18}O_{Qtz-Mt}$ fractionations for the samples furthest from the contact (>2.6 km, isograd zone 2) indicates that these samples never achieved isotopic equilibrium.

Evidence for oxygen isotope exchange during cooling

Interpretation of the apparent quartz–magnetite temperatures as reset requires consideration of the oxygen diffusion

domains. Because oxygen diffusion is slower in magnetite than quartz (Giletti and Hess 1988; Cole and Chakraborty 2001), and the $\delta^{18}O$ values for magnetite are more variable than those of quartz (Table S6), we would expect that the rate-limiting step for retrograde oxygen isotope exchange lies in oxygen diffusion in magnetite (see Valley 2001). If this interpretation is correct, the maximum metamorphic temperatures were higher than the apparent temperatures calculated by quartz–magnetite oxygen isotope thermometry. Such a conclusion is consistent with the fact that metamorphic temperatures calculated from inverted pigeonite at Dunka Pit are more than 100°C higher than the apparent quartz–magnetite oxygen isotope temperatures.

We use magnetite as the basis for considering diffusion distances of oxygen (Giletti and Hess 1988). For thin sections of samples near the gabbro contact at Dunka Pit, the magnetite grain radius is taken as the diffusion distance and was measured by petrographic microscope. For the rest of the samples, representative grain size was estimated from back-scattered electron images. In samples where the magnetite-rich layers were primarily composed of magnetite (>80%), the half width of the magnetite layer was considered to be the diffusion distance. These results are summarized in Table S9.

In Fig. 7 we compare the apparent quartz–magnetite O isotope temperatures with calculated closure temperatures (T_c) based on oxygen diffusion in magnetite. Closure temperatures are calculated using the Dodson (1973) equation:

$$T_c = \frac{(E/R)}{ln\left\{\frac{-A \cdot R \cdot T_c^2 (D_o/a^2)}{E\left(\frac{\delta T}{\delta t}\right)}\right\}} \tag{7}$$

where A = diffusional anisotropy parameter (55 for magnetite, 8.7 for quartz), a = diffusion distance, nominally the radius of the mineral grain (in cm), R = the gas constant (J/mol K), D_o = pre-exponential factor (cm²/s), E = activation energy (J/mol), and $\delta T/\delta t$ = linear cooling rate (K/s). Using the oxygen diffusion coefficient in magnetite at $P(H_2O) = 1$ kb of Giletti and Hess (1988), a cooling rate of 5.6°C/kyr, T_c is 700°C for 0.6 mm (radius) magnetite, which is a typical grain size for the Upper Cherty unit rocks at the contact with the Duluth Complex. The apparent temperature of 918°C for the xenolith likely reflects a locally dry environment, which could cause slow diffusion of oxygen in magnetite and quartz. The closure temperature calculated for hydrothermal quartz (Dennis 1984) at the contact is 618°C, which is ~80°C lower than that of magnetite. Other primary minerals at the contact are pyroxene and fayalite. These minerals diffuse oxygen more slowly than quartz (Fortier and Giletti 1989; Zheng and Fu 1998; Cole and Chakraborty 2001). We may therefore
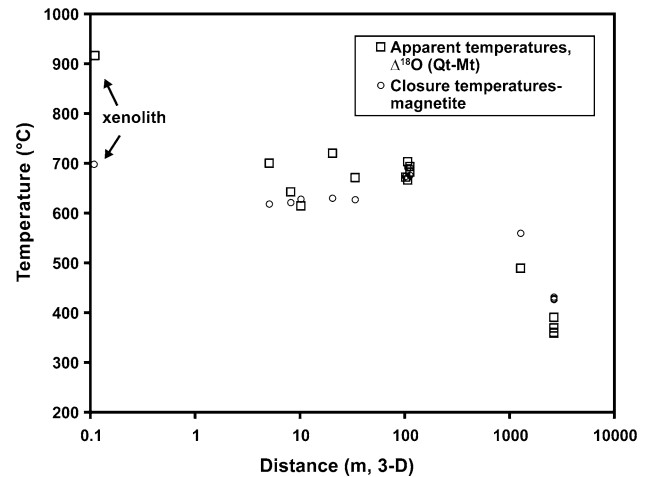

Fig. 7 Comparison of apparent O isotope temperatures and the closure temperatures predicted from the Dodson equation as applied to O diffusion in magnetite with a cooling rate of 5.6°C/kyr. Closure temperature decreases away from the contact due to smaller crystal size. Data from Tables S6 and S9

safely assume that, in the absence of fluid flow, there is no exchangeable reservoir other than quartz at temperatures below T_c of magnetite. Therefore, the magnetite T_c reflects the closure temperature of the quartz–magnetite fractionation.

With the exception of three samples within 100 m of the contact, the calculated closure temperatures are similar to the apparent quartz–magnetite temperatures (Fig. 7; Table S9). If apparent temperatures are less than peak temperatures, the $\delta^{18}O$ values for magnetite should vary with grain size. To test this hypothesis, magnetite was sieved from two samples, 03BIW43B (5 m from contact) and 03BIW18C (8 m), from Dunka Pit (Table S10). Two grain diameters were separated for single crystals of magnetite, 500–350 and 150–105 μm. Unbroken crystals of each size range were hand-picked and analyzed for $\delta^{18}O$, and apparent quartz–magnetite oxygen isotope temperatures were calculated using matrix quartz. Because oxygen diffusion is faster in quartz, it is assumed to have become homogenized during cooling below T_c(Mt). For sample 03BIW43B, the bulk magnetite separate produced an apparent quartz–magnetite temperature of 702°C (average grain size: 197 μm; Table S9). The large magnetite fraction (350–500 μm) produced a higher apparent temperature of 716°C, and, most importantly, the small fraction (105–150 μm) produced the lowest apparent temperature of 669°C (Table S10). Similar results were found for sample 03BIW18C, where the bulk separate (average grain size: 205 μm; Table S9) produced an apparent temperature of 644°C, the larger size fraction produced 732°C, and the smaller size fraction produced 601°C (Table S10). These temperatures compare with those calculated from the Dodson equation (Eq. 7), where, assuming a cooling rate of
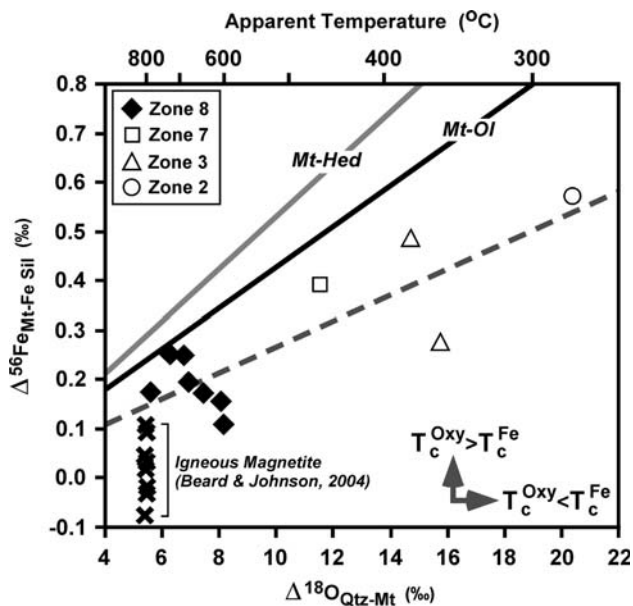
Fig. 8 Measured $\Delta^{56}Fe_{Mt\text{-}Fe\ Sil}$ fractionations versus measured $\Delta^{18}O_{Qtz\text{-}Mt}$ fractionations. *Temperature scale* shown at *top* corresponds to apparently reset oxygen isotope fractionations. Also shown are $\Delta^{56}Fe_{Mt\text{-}Fe\ Sil}$ fractionations measured in quickly cooled volcanic rocks, plotted against crystallization temperature using Fe–Ti oxide thermometry (Beard and Johnson 2004). *Diagonal lines* are the predicted magnetite–hedenbergite and magnetite–olivine Fe isotope fractionations from Polyakov and Mineev (2000) and Polyakov et al. (2007), combined with the measured quartz–magnetite O isotope fractionations. Regression of the measured fractionations produces $\Delta^{56}Fe_{Mt\text{-}Fe\ Sil} = 0.168\ (10^6/T^2)$ (*T* in K), with an R^2 of 0.70 (*dashed line*). *Arrows* mark relative trajectories for deviation from the predicted O–Fe isotope fractionations, depending upon the relative closure temperatures for O (T_C^{Oxy}) and Fe (T_C^{Fe}). Data from Tables S6 and S8

5.6°C/kyr, the difference in T_c between a 450 μm crystal (625°C) and a 128 μm (552°C) is 73°C. The data for the different size fractions are therefore broadly consistent with the interpretation that the quartz–magnetite oxygen isotope temperatures reflect exchange by diffusion during cooling, and not peak temperatures of metamorphism.

Fe isotope fractionations

Quartz–magnetite O isotope fractionations ($\Delta^{18}O_{Qtz\text{-}Mt}$) are positively correlated with magnetite–Fe silicate Fe isotope fractionations ($\Delta^{56}Fe_{Mt\text{-}Fe\ Sil}$), suggesting that both isotope systems record the effects of metamorphism (Fig. 8). Frost et al. (2007) observed that their measured $\Delta^{56}Fe_{Mt\text{-}Fe\ Sil}$ fractionations in the Biwabik Iron Formation did not follow those predicted for coexisting magnetite–olivine or magnetite–hedenbergite (Polyakov and Mineev 2000; Polyakov et al. 2007) based on their estimated metamorphic temperatures, and they interpreted this to reflect a lack of Fe isotope equilibrium among magnetite and Fe silicates during

metamorphism. Indeed, our measured $\Delta^{18}O_{Qtz\text{-}Mt} - \Delta^{56}Fe_{Mt\text{-}Fe\ Sil}$ fractionations do not lie along the predicted O–Fe trend, using the $\Delta^{18}O_{Qtz\text{-}Mt}$ versus temperature relations of Clayton and Kieffer (1991), and $\Delta^{56}Fe_{Mt\text{-}Olivine}$ or $\Delta^{56}Fe_{Mt\text{-}Hedenbergite}$ versus temperature relations of Polyakov and Mineev (2000) and Polyakov et al. (2007) (Fig. 8).

We interpret the $\Delta^{18}O_{Qtz\text{-}Mt} - \Delta^{56}Fe_{Mt\text{-}Fe\ Sil}$ relations in Fig. 8 to reflect attainment of O and Fe isotope equilibrium in at least zone 8, followed by cooling through the closure temperatures for O and Fe, $T_C^{Oxy} < T_C^{Fe}$. This contrasts with the interpretation of Fe isotope fractionations by Frost et al. (2007), who argued that any temperature dependence in magnetite–Fe silicate fractionations was fortuitous. As noted above, T_C^{Oxy} for magnetite is generally less than $\sim650°C$ in zone 8, significantly less than the $\geq800°C$ peak temperatures predicted by a conductive cooling model for ≤100 m from the contact (Figs. 6, 7). Based on the diffusion data for oxygen in magnetite (Giletti and Hess 1988), and iron in magnetite (Freer and Hauptman 1978) and olivine (Chakraborty 1997), the relative closure temperatures should be olivine (Fe) > magnetite (O) > magnetite (Fe); this is the same relative order estimated by Frost et al. (2007), who calculated the closure temperature for Fe silicates was $\sim730°C$ for the Biwabik Iron Formation based on an assumed cooling rate of 0.7–2°C/kyr and grain size of 1 mm. However, even this high closure temperature is below the peak metamorphic temperatures of zone 8 (Fig. 6), which supports the interpretation that the correlation between $\Delta^{18}O_{Qtz\text{-}Mt}$ and $\Delta^{56}Fe_{Mt\text{-}Fe\ Sil}$ (Fig. 8) reflects isotopic exchange during metamorphism. The offset in the measured fractionations relative to the O and Fe isotope thermometers likely reflects, at least in part, the higher closure temperatures for Fe (constrained by the Fe silicates) relative to O (constrained by magnetite). The scatter in the $\Delta^{18}O_{Qtz\text{-}Mt} - \Delta^{56}Fe_{Mt\text{-}Fe\ Sil}$ relations may reflect the fact that our Fe silicate separates (made by physical separation) contain mixtures of different silicates, given the difference in predicted magnetite–olivine and magnetite–hedenbergite Fe isotope fractionations (Fig. 8).

Our results suggest that the equilibrium magnetite–Fe silicate Fe isotope fractionation at ~750–$800°C$ is $\sim+0.2‰$, using the samples that had the smallest quartz–magnetite oxygen isotope fractionations (Fig. 8). This is identical to the magnetite–Fe silicate fractionation measured by Frost et al. (2007) for their highest grade sample, as well as a magnetite–pyroxene pair from the high-grade Isua BIFs analyzed by Dauphas et al. (2004). These fractionations are, however, significantly higher than the near-zero magnetite–Fe silicate fractionations at $\sim800°C$ measured by Beard and Johnson (2004) in quenched volcanic rocks. We speculate that this contrast reflects the different chemical compositions for igneous magnetite relative to magnetite from the Biwabik Iron Formation. In igneous rocks, Al, Cr, Mn^{3+}, and Ti^{4+} may

substitute for Fe^{3+} in magnetite, where the most common substitution is Ti as part of the magnetite–ulvöspinel solid solution that exists at magmatic temperatures. The igneous magnetites analyzed by Beard and Johnson (2004) (Fig. 8) contained 4.7–5.5 wt% TiO_2, 1.4–1.8 wt% Al_2O_3, 0.6–0.7 wt% MnO, and 0.8–1.1 wt% MgO. In contrast, magnetite in the contact metamorphic zone of Gunflint Iron Formation, which is correlative with the Biwabik Iron Formation, is near end member Fe_3O_4, where TiO_2 contents are <0.1 wt% except in a few samples reported from near the contact (Floran and Papike 1978; Muhich 1993). Polyakov and Mineev (2000) noted that element substitution for Fe^{3+} may affect the reduced partition function ratio of magnetite ($\beta_{56/54}$), although they did not calculate the effects of Ti substitution. The contrasting Fe isotope fractionations in the Biwabik and igneous rocks, as well as the fact that the Ti-bearing magnetite in igneous rocks did not produce fractionations that overlap those predicted by Polyakov and Mineev (2000) and Polyakov et al. (2007), suggests that effects on the order of a few tenths per mil in $^{56}Fe/^{54}Fe$ ratios for magnetite may occur due to variations in magnetite composition.

Open- and closed-system exchange of O and Fe isotopes

Covariations between $\delta^{18}O_{Qtz}$ and $\delta^{18}O_{Mt}$ suggest two different responses to metamorphism as a function of distance to the contact. Most of the data lie within the envelope of closed system isotopic exchange defined by the molar oxygen quartz/magnetite ratios (Fig. 9; see, Gregory et al. 1989). The $\delta^{18}O$ values for the primary iron oxide-bearing sediments and lowest-grade metamorphic equivalents will plot to the right (below) the 300°C isopleth (Fig. 9). The relatively large range in $\delta^{18}O_{Mt}$ relative to $\delta^{18}O_{Qtz}$ is consistent with the relatively high molar oxygen quartz/magnetite ratio, which ranges from 0.42 to 3.61. The data for the outer part of the contact aureole (>200 m) scatter about a negative slope that may suggest partial isotopic re-equilibration along molar oxygen quartz/magnetite ratios that lie within the range observed for the samples. The data within 200 m of the contact, however, scatter about a high-temperature isopleth and are positively correlated, which suggests local exchange with low $\delta^{18}O$ magmatic water from the Duluth Complex, or variability in the initial bulk-sample $\delta^{18}O$ values.

Calculated $\delta^{18}O_{WR}$ values (Table S3) scatter between +10 and +15‰ (Fig. 4). The average $\delta^{18}O_{WR}$ value is 11.9 ± 0.6‰ for samples within 33 m of the contact at Dunka Pit, 12.6 ± 1.0‰ outside Dunka Pit but less than 2.6 km from the contact, and 12.9 ±2.6‰ for samples greater than 2.6 km from the contact. These $\delta^{18}O_{WR}$ values are suggestive of some fluid infiltration with proximity to

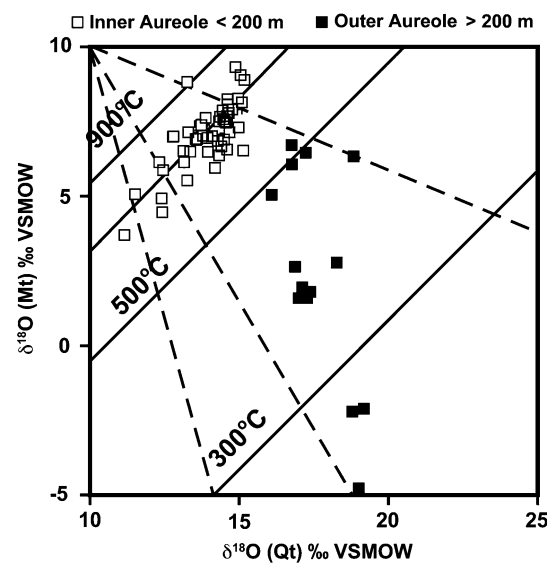**Fig. 9** Variations in $\delta^{18}O_{Qtz}$ and $\delta^{18}O_{Mt}$ values in the Biwabik rocks. Equilibrium temperatures (*solid diagonal lines*) from Clayton and Kieffer (1991). The analytical uncertainty is less than the size of the *symbols*. *Dashed lines* show the trajectories expected for closed system isotopic exchange between quartz and magnetite using the average, maximum, and minimum molar O quartz/magnetite ratios. The relatively large changes in $\delta^{18}O_{Mt}$ values as compared to $\delta^{18}O_{Qtz}$ reflects the relatively low magnetite abundances as compared to quartz. Note that some samples near the contact plot to the *left* of the trajectory of lower temperature samples suggesting open system exchange with lower $\delta^{18}O$ fluids. Data from Table S6

the contact, although they overlap within the scatter of the data. Independent evidence for fluid exchange at the contact lies in the chemical composition of magnetite, which is nearly end-member Fe_3O_4 away from the contact, but is enriched in Ti with proximity to the Duluth Complex, reflecting ulvöspinel solid-solution in magnetite (Muhich 1993). Metasomatic alteration of the Biwabik Iron Formation with proximity to the contact is also indicated by increases in Al and alkalis (Muhich 1993).

In the absence of significant fluid flow, in principle, the premetamorphic $\delta^{18}O_{Mt}$ and $\delta^{18}O_{Qtz}$ values may be estimated through extrapolation to low-temperature quartz–magnetite fractionation lines (<300°C; Fig. 9) along the molar O quartz/magnetite ratios for individual samples. Such an approach assumes a closed-system and does not account for changes in magnetite and quartz proportions during metamorphism. Despite these issues, however, it is clear that the pre-metamorphic $\delta^{18}O$ values for magnetite (or their oxide precursors) must have been lower (Fig. 9). Using the range of molar O quartz/magnetite ratios in the samples, the low-temperature $\delta^{18}O_{Mt}$ values probably ranged from –6 to +1‰, and the $\delta^{18}O_{Qtz}$ values were probably in the range of +20 to 25‰.

The relations between the $\delta^{56}Fe$ values for magnetite and Fe silicates, and the calculated whole-rock $\delta^{56}Fe$
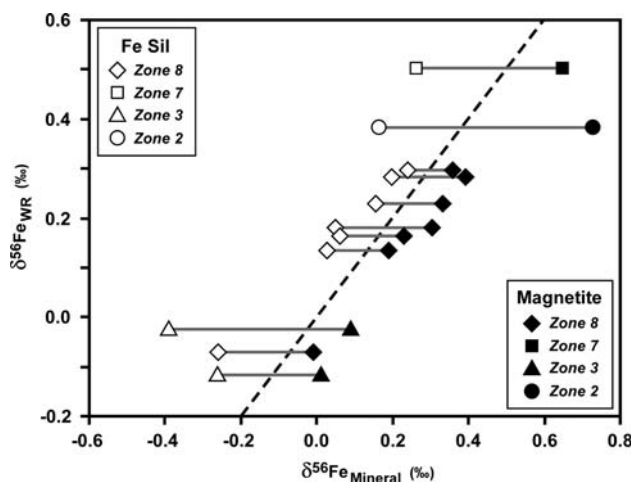
Fig. 10 Variation in $\delta^{56}Fe_{Mt}$ and $\delta^{56}Fe_{Fe\ Sil}$ values as a function of calculated whole-rock (WR) $\delta^{56}Fe$ values. A 1:1 reference line (*dashed*) shows the Fe isotope mass-balance control of the whole-rock relative to magnetite and Fe silicate. Although the magnetite–Fe silicate fractionation varies with temperature (Fig. 8), there is no correlation with calculated $\delta^{56}Fe_{WR}$ values, suggesting that the bulk Fe isotope compositions were not homogenized from zone to zone during metamorphism. Data from Tables S4 and S8

Fig. 11 Co-variation in $\delta^{18}O_{Mt}$ and $\delta^{56}Fe_{Mt}$ values and isotope exchange trajectories that would be produced by metamorphism. *Solid lines* indicate coupled O–Fe isotope exchange in a closed system at two different whole-rock Fe isotope compositions (*left line* $\delta^{18}O_{WR} = +13‰$, $\delta^{56}Fe_{WR} = -0.2‰$; *right line* $\delta^{18}O_{WR} = +13‰$, $\delta^{56}Fe_{WR} = +0.5‰$), as calculated using Eqs. 8 and 9 in the text and the average molar O/Fe ratio of the samples. The trajectories are only slightly changed if the minimum or maximum molar O/Fe ratios in the Biwabik samples are used. O–Fe isotope exchange is assumed to have occurred via the relation $\Delta^{56}Fe_{Mt-Fe\ Sil} = 0.0255\ \Delta^{18}O_{Qtz-Mt}$, equivalent to the regression of the measured O and Fe isotope fractionations (*dashed line* in Fig. 8). These relations indicate that the low-temperature $\delta^{18}O_{Mt}$ values were at least 10‰ lower than those measured in the high-grade portions of the Biwabik Iron Formation, and the low-temperature $\delta^{56}Fe_{Mt}$ values were $\sim$0.3‰ higher than those in the high-temperature samples, assuming closed-system isotopic exchange at constant mineral abundances

values based on modal abundances, demonstrate the mass-balance control between the Fe silicates and magnetite (Fig. 10). In all cases, the $\delta^{56}Fe$ values of the Fe silicates are lower than those of the coexisting magnetite. This relation was generally observed by Frost et al. (2007), but in some cases they found magnetite–Fe silicate reversals, which they argued reflect primary, low-temperature compositions that did not equilibrate during metamorphism. In contrast, we argue that the Fe isotope fractionations between magnetite and Fe silicate are a function of metamorphic grade (Figs. 8, 10), an interpretation supported by the evidence discussed above that peak metamorphic temperatures exceeded the closure temperatures of O and Fe. That there is no correlation between calculated bulk $\delta^{56}Fe$ value and metamorphic grade (Figs. 4, 10) indicates that widespread Fe isotope homogenization did not occur. The bulk $\delta^{56}Fe$ values for individual BIF layers, therefore, seem likely to have been preserved despite high-grade metamorphism, a conclusion Frost et al. (2007) reached in their Fe isotope study of the Biwabik Iron Formation, and one with which we agree.

Co-variations between the measured $\delta^{18}O_{Mt}$ and $\delta^{56}Fe_{Mt}$ values demonstrate the distinct trajectories for O and Fe that are expected for isotopic equilibration during metamorphism. Because oxygen isotope fractionations are more sensitive to variations in temperature than iron isotope fractionations, and because magnetite comprises a relatively small oxygen inventory, but the major iron inventory, $\delta^{18}O_{Mt}$ values changed over 10‰ during metamorphism of the Biwabik Iron Formation, but $\delta^{56}Fe_{Mt}$
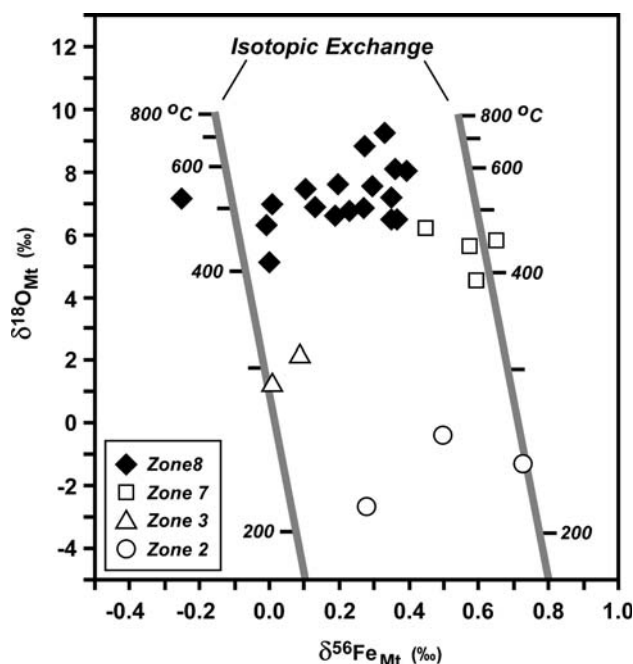
values are predicted to change by only $\sim$0.3‰ (Fig. 11). The effects of isotopic equilibration during metamorphism were calculated using the mass-balance equations:

$$\delta^{56}Fe_{Mt} = \delta^{56}Fe_{WR} - \Delta^{56}Fe_{Mt-Fe-Sil}(X_{Mt-1}) \qquad (8)$$

and

$$\delta^{18}O_{Mt} = \delta^{18}O_{WR} + \Delta^{18}O_{Qtz-Mt}(X_{Mt-1}) \qquad (9)$$

where the whole-rock $\delta^{56}Fe$ and $\delta^{18}O$ values fix the relative position of the equilibration curves, X_{Mt} is the Fe or O mole fraction in a simple two-component magnetite–Fe silicate or magnetite–quartz mixture, respectively, and the temperature dependence of $\Delta^{56}Fe_{Mt-Fe\ Sil}$ and $\Delta^{18}O_{Qtz-Mt}$ are from regression of the measured results in Fig. 8. Extrapolating to the $\delta^{56}Fe_{Mt}$ or $\delta^{18}O_{Mt}$ variations expected at low temperatures indicates that the $\delta^{56}Fe_{Mt}$ values for

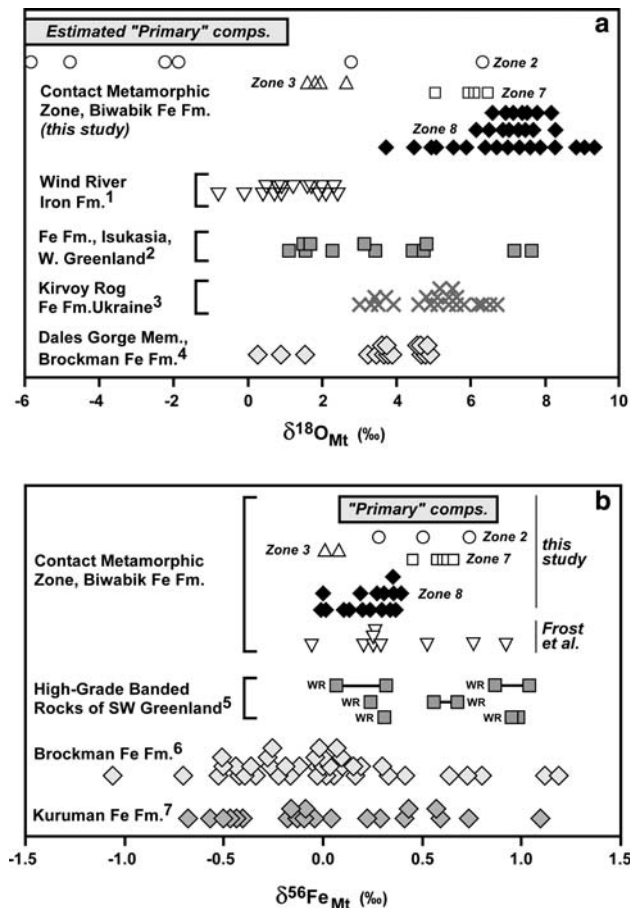**Fig. 12** Comparison of $\delta^{18}O$ and $\delta^{56}Fe$ values for magnetite from banded Iron Formations from around the world. *Horizontal bars* indicate estimated low-temperature, "primary" O and Fe isotope compositions, based on closed-system exchange model in Fig. 11. Data sources: *1* Sharp et al. (1988); *2* Perry et al. (1978); *3* Perry and Ahmad (1981); *4* Becker and Clayton (1976); *5* Dauphas et al. (2004); *6* Johnson et al. (2007); *7* Johnson et al. (2003)

the initial low-temperature magnetite was ~0.3‰ higher than those measured for the highest-grade samples. This contrasts with the interpretation of Frost et al. (2007) that the measured $\delta^{56}Fe_{Mt}$ values directly record the low-temperature, "primary" compositions.

Comparison with O and Fe isotope data from other banded iron formations

The largest range in $\delta^{18}O$ and $\delta^{56}Fe$ values for magnetite from BIFs tends to be found in the lowest-grade samples that have been studied to date (Fig. 12). The effects of metamorphism produce a strong increase in $\delta^{18}O_{Mt}$ values and slight decrease in $\delta^{56}Fe_{Mt}$ values (Fig. 11). Magnetite from isograd zone 2 ranges in $\delta^{18}O$ from approximately –6 to +6‰, reflecting equilibration with seawater or low-$\delta^{18}O$ pore fluids during deposition, as well as exchange at

moderate metamorphic grade. The estimated low-temperature isotopic compositions have a slightly more restricted range in $\delta^{18}O_{Mt}$ values, ~–6 to +1‰. The Biwabik Iron Formation data overlap all $\delta^{18}O_{Mt}$ values determined from other BIFs (Fig. 12). Of the BIFs that have been previously analyzed for O isotope compositions, zone 2 of the Biwabik Iron Formation and the Dales Gorge Member of the Brockman Iron Formation experienced the lowest grades of metamorphism (sub-greenschist facies; Becker and Clayton 1976; this study). The Kirvoy Rog Iron Formation (greenschist- to amphibolite-facies), the Iron Formation in Isukasia in Western Greenland (amphibolite-facies), and the Wind River Iron Formation (granulite-facies) define a range in $\delta^{18}O_{Mt}$ values that overlaps those of the contact metamorphosed Biwabik Iron Formation. We suggest that the higher $\delta^{18}O_{Mt}$ values in this range reflect the greatest extent of metamorphic equilibration, but this is difficult to assess without detailed knowledge of the molar O magnetite/silicate ratios in the rocks.

The lowest-grade BIFs also have the largest range in $\delta^{56}Fe$ values (Fig. 12), including the Kuruman Iron Formation, which was metamorphosed to ~100–200°C, and the Dales Gorge member of the Brockman Iron Formation, which was metamorphosed to ~300°C (Becker and Clayton 1976; Johnson et al. 2003). Curiously, none of the magnetite from the zone 2 isograd samples in this study, nor the estimated low-temperature isotopic compositions (Fig. 11), have the low $\delta^{56}Fe$ values that are common in the Kuruman and Dales Gorge units (Fig. 12). The positive $\delta^{56}Fe_{Mt}$ values of the Biwabik Iron Formation are similar to those found in the 3.7 Ga Isua BIFs (Fig. 12), but these do not reflect metamorphism because metamorphic equilibration will tend to decrease $\delta^{56}Fe_{Mt}$ values if Fe silicates were also present (Fig. 11). Instead, Johnson et al. (2008) suggest that the positive $\delta^{56}Fe_{Mt}$ values for the 3.7 and 1.8 Ga BIFs may reflect a lack of bacterial iron reduction at these time periods.

Conclusions

The thermal gradients that were imposed on the 1.9 Ga Biwabik Iron Formation by the 1.1 Ga Duluth gabbro intrusions produced systematic changes in O and Fe isotope fractionations between coexisting minerals. The minimum temperatures recorded by pigeonite stability in Biwabik rocks near the contact, as well as estimated intrusion temperatures for the Duluth Complex, produce thermal profiles that indicate peak metamorphic temperatures greater than the apparent quartz–magnetite oxygen isotope temperatures. Estimated closure temperatures for O in magnetite are similar to the apparent O isotope temperatures, suggesting that the quartz–magnetite O isotope

fractionations reflect oxygen exchange by diffusion upon cooling, where Biwabik rocks near the contact cooled at ~5.6°C/kyr. At this rate, the Biwabik Iron Formation at the contact cooled from ~825 to 400°C in ~75 kyr. This interpretation is supported by a correlation of apparent quartz–magnetite O isotope temperatures with magnetite grain size.

Comparison of quartz–magnetite O isotope fractionations with magnetite–Fe silicate Fe isotope fractionations suggest that both reflect the effects of metamorphism, and this is supported by recognition that peak metamorphism exceeded the closure temperatures for O and Fe. Extrapolation to pre-metamorphic conditions indicates that the "original" $\delta^{18}O$ values for magnetite were at least 10‰ lower, and quartz were at least 5‰ higher, than those in the higher-grade portions of the contact aureole. Because a relatively large proportion of the Fe inventory lies in magnetite, coupled with the relatively smaller Fe isotope fractionations, the shift in Fe isotope compositions of magnetite during metamorphism was much smaller. The $\delta^{56}Fe$ values for magnetite at pre-metamorphic conditions were ~0.3‰ higher than those in the high-grade Biwabik rocks. Because the effects of metamorphism decrease $\delta^{56}Fe_{Mt}$ values in rocks that also contain Fe silicates, metamorphism cannot explain the positive $\delta^{56}Fe_{Mt}$ values measured in the 1.8 Ga Biwabik BIFs, as well as Early Archean BIFs, and such values may reflect changes in the biogeochemical cycles of Fe relative to those involved in the intermediate-age (~2.5 Ga) BIFs (Johnson et al. 2008).

References

Albaréde F, Beard BL (2004) Analytical methods for non-traditional isotopes, In: Johnson CM, Beard BL, Albaréde F (eds) Geochemistry of non-traditional stable isotopes reviews in mineralogy and geochemistry, vol 56. Mineralogical Society of America, Washington D.C., pp 113–152

Beard BL, Johnson CM (2004) Inter-mineral Fe isotope variations in mantle derived rocks and implications for the Fe geochemical cycle. Geochim Cosmochim Acta 68:4727–4743

Beard BL, Johnson CM, Skulan JL, Nealson KH, Cox L, Sun H (2003) Application of Fe isotopes to tracing the geochemical and biological cycling of Fe. Chem Geol 195:87–117

Becker RH, Clayton RN (1976) Oxygen isotope study of a precambrian banded iron-formation, Hamersley Range, Western Australia. Geochim Cosmochim Acta 40:1153–1165

Bonnichsen B (1969) Metamorphic pyroxenes and amphiboles in the Biwabik iron formation, Dunka River area, Minnesota, Mineralogical Society of America, Special Paper 2, pp 217–239

Bonnichsen B (1972) Southern part of the Duluth Complex, Geology of Minnesota: a Centennial Volume. Sims PK, Morey GB (eds), pp 361–388

Bonnichsen B (1975) Geology of the Biwabik iron formation, Dunka River Area, Minnesota. Econ Geol 70:319–340

Chalokwu CI, Grant NK, Ariskin AA, Barmina GS (1993) Simulation of primary phase relations and mineral compositions in the Partridge River intrusion, Duluth Complex, Minnesota: implications for the parent magma composition. Contrib Mineral Petrol 114:539–549

Chakraborty S (1997) Rates and mechanisms of Fe–Mg interdiffusion in olivine at 980–1300°C. J Geophys Res 102:12317–12331

Clayton RN, Kieffer SW (1991) Oxygen isotopic thermometer calibrations. In: Taylor HP, O'Neil JR, Kaplan IR (eds) Geochemical Society Special Publication, vol 3, pp 3–10

Cloud PE, Jr (1968) Atmospheric and hydrospheric evolution on the primitive Earth. Science 160(3829):729–736

Cole DR, Chakraborty S (2001) Rates and mechanisms of isotopic exchange. In: Valley JW, Cole DR (eds) Mineralogical Society of America Reviews in Mineralogy and Geochemistry, vol 43, pp 365–413

Dauphas N, van Zuilen M, Wadhwa M, Davis AM, Marty B, Janney PE (2004) Clues from Fe isotope variations on the origin of Early Archean BIFs from Greenland. Science 306:2077–2080

Dauphas N, Cates NL, Mojzsis SJ, Busigny V (2007) Identification of sedimentary protoliths using iron isotopes in the >3700 Ma Nuvvuagittuq supracrustal belt, Canada. Earth Planet Sci Lett 254:358–376

Dennis PF (1984) Oxygen self diffusion in quartz under hydrothermal conditions. J Geophys Res 89:4047–4057

Dodson MH (1973) Closure temperature in cooling ages. Contrib Mineral Petrol 40:259–274

Floran RJ, Papike JJ (1978) Mineralogy and petrology of the Gunflint iron formation, Minnesota-Ontario: correlation of compositional and assemblage variations at low to moderate grade. J Petrol 19:215–288

Fortier SM, Giletti BJ (1989) An empirical model for predicting diffusion coefficients in silicate minerals. Science 245:1481–1484

Fralick P, Davis DW, Kissin SA (2002) The age of the Gunflint Formation, Ontario, Canada: single zircon U–Pb age determinations from reworked volcanic ash. Can J Earth Sci 39:1085–1091

Freer R, Hauptman Z (1978) An experimental study of magnetite–titanomagnetite interdiffusion. Phys Earth Planet Inter 16:223–231

French BM (1968) Progressive contact metamorphism of the Biwabik iron formation, Mesabi Range, Minnesota. Minn Geol Surv Bull 45:1–103

Frost CD, von Blanckenburg F, Schoenberg R, Frost BR, Swapp SM (2007) Preservation of Fe isotope heterogeneities during diagenesis and metamorphism of banded iron formation. Contrib Mineral Petrol 153:211–235

Giletti BJ, Hess KC (1988) Oxygen diffusion in magnetite. Earth Planet Sci Lett 89:115–122

Gregory RT, Criss RE, Taylor HP (1989) Oxygen isotope exchange kinetics of mineral pairs in closed and open systems: applications to problems of hydrothermal alteration of igneous rocks and Precambrian iron formations. Chem Geol 75:1–42

Gundersen JN, Schwartz GM (1962) The geology of the metamorphosed Biwabik iron formation, Eastern Mesabi district, Minnesota. Minn Geol Surv Bull 43:1–139

Hauck SA, Severson MJ, Zanko L, Barnes SJ, Morton P, Alminas H, Foord E, Dahlberg EH (1997) An overview of the geology and oxide, sulfide and platinum-group element mineralization along

the western and northern contacts of the Duluth Complex. Geol Soc Am Spec Pap 312:137–185

Hemming SR, McLennan SM, Hanson GN (1996) Geochemical source characteristics and diagenetic trends of the Virginia Formation, Mesabi Iron Range, Minnesota. Institute on Lake Superior Geology Proceedings, 42nd Annual Meeting, Cable WI, 1996; v. 42, pt. 1:13 (abstract)

Jaeger JC (1957) The temperature in the neighborhood of a cooling intrusive sheet. Am J Sci 255:306–318

Jaeger JC (1959) Temperatures outside a cooling intrusive sheet. Am J Sci 257:44–54

Johnson CM, Beard BL, Beukes NJ, Klein C, O'Leary JM (2003) Ancient geochemical cycling in the earth as inferred from Fe isotope studies of banded iron formations from the Transvaal Craton. Contrib Mineral Petrol 144:523–547

Johnson C, Beard B, Roden E, Newman D, Nealson K (2004) Isotopic constraints on biogeochemical cycling of Fe. In reviews in mineralogy and geochemistry: geochemistry of non-traditional stable isotopes, vol 55, pp 359–408

Johnson CM, Roden EE, Welch SA, Beard BL (2005) Experimental constraints on Fe isotope fractionation during magnetite and Fe carbonate formation coupled to dissimilatory hydrous ferric oxide reduction. Geochim Cosmochim Acta 69:963–993

Johnson CM, Beard BL, Klein C, Beukes NJ, Roden EE (2007) Iron isotopes constrain biologic and abiologic processes in banded iron formation genesis. Geochim Cosmochim Acta (in press)

Johnson CM, Beard BL, Roden EE (2008) The iron isotope fingerprints of redox and biogeochemical cycling in the modern and ancient Earth. Annu Rev Earth Planet Sci (in press)

Knauth LP, Lowe DR (2003) High Archean climatic temperature inferred from oxygen isotope geochemistry of cherts in the 3.5 Ga Swaziland Supergroup, South Africa. Geol Soc Am Bull 115:566–580

Koptev-Dornikov EV, Chalokwu CI, Arskin AA, Grant NK (1995) Forward modeling of incompatible element enrichment in the basal zone of the Partridge River intrusion, Eos, Transactions, American Geophysical Union, vol 76 supplement, p 288

Lindsley DH (1983) Pyroxene thermometry. Am Mineral 68:477–493

Miyano T, Klein C (1986) Fluid behavior and phase relations in the system Fe–Mg–Si–C–O–H: application to high grade metamorphism of iron-formations. Am J Sci 286:540–575

Morey GB (1983) Animikie Basin, lake superior region. In: Trendall AF, Morris RC (eds) Iron-formation: facts and problems, pp 13–67

Morey GB (1992) Chemical composition of the Eastern Biwabik iron-formation (Early Proterozoic), Mesabi Range, Minnesota. Econ Geol 87:1649–1658

Morey GB and van Schmus (1988) Correlation of precambrian rocks of the lake superior region United States. U.S.G.S. Prof. Pap. 1241-F, 31p

Morey GB, Papike JJ, Smith RW, Weiblen PW (1972) Observations on the contact metamorphism of the Biwabik iron-formation, east Mesabi district, Minnesota. Geol Soc Am Mem 135:225–263

Muhich TG (1993) Diffusion of Ti across the Duluth Complex-Biwabik iron formation contact at Dunka Pit, Mesabi Iron Range, Northeastern Minnesota. Geol Soc Am Abstr Programs 25:69

Ojakangas RW, Severson MJ, Jongewaard PK, Arola JL, Evers JT, Valverson DG, Morey GB, Holst TB (2005) Geology and sedimentology of the Paleoproterozoic Animikie Group: the Pokegama Formation, the Biwakiki Iron Formation, and Virginia

Formation of the eastern Mesabi Iron Range and the Thompson Formation near Duluth, northeastern Minnesota. In: Robinson L (ed) Field trip guidebook for selected geology in Minnesota and Wisconsin. Minnesota Geological Survey Guidebook 21:214–243

Perry EC, Ahmad SN (1981) Oxygen and carbon isotope geochemistry of the Krivoy Rog iron formation. Urkranian SSR. Lithos 14:83–92

Perry EC, Bonnichsen B (1966) Quartz and magnetite: oxygen 18-oxygen 16 fractionation in metamorphosed Biwabik formation. Science 153:528–529

Perry EC, Lefticariu L (2003) Formation and geochemistry of Precambrian cherts. Holland H, Turekian K (eds) Treatise on Geochemistry, vol 7, pp 99–113

Perry EC, Tan FC (1972) Significance of oxygen and carbon isotope variations in early Precambrian cherts and carbonate rocks of Southern Africa. Geol Soc Am Bull 83:647–664

Perry EC, Tan FC, Morey GB (1973) Geology and stable isotope chemistry of the Biwabik iron formation, northern Minnesota. Econ Geol 68:1110–1125

Perry EC, Ahmad SN, Swulius TM (1978) The oxygen isotope composition of 3800 M.Y. old metamorphosed chert and iron formation from Isukasia, West Greenland. J Geol 86:223–239

Polyakov VB, Mineev SD (2000) The use of Mössbauer spectroscopy in stable isotope geochemistry. Geochim Cosmochim Acta 64:849–865

Polyakov VB, Clayton RN, Horita J, Mineev SD (2007) Equilibrium iron isotope fractionation factors of minerals: reevaluation from the data of nuclear inelastic resonant X-ray scattering and Mössbauer spectroscopy. Geochim Cosmochim Acta 71:3833–3846

Sharp ZD, O'Neil JR, Essene EJ (1988) Oxygen isotope variations in granulite-grade iron formations: constraints on oxygen diffusion and retrograde isotopic exchange. Contrib Mineral Petrol 98:490–501

Simmons EC, Lindsley DH, Papike JJ (1974) Phase relations and crystallization sequence in contact-metamorphosed rock from the Gunflint Iron Formation, Minnesota. J Petrol 15:539–565

Spicuzza MJ, Valley JW, Kohn MJ, Girard JP, Fouillac AM (1998) The rapid heating, defocused beam technique; a CO_2 laser-based method for highly precise and accurate determination of $\delta^{18}O$ values of quartz. Chem Geol 144:195–203

Stookey LC (1970) Ferrozine—a new spectrophotometric reagent from iron. Anal Chem 42:779–781

Valaas EP (2004) Oxygen isotope thermometry in contact metamorphosed Biwabik iron-formation. MS thesis, University of Wisconsin-Madison, p 65

Valley JW (2001) Stable isotope thermometry at high temperatures: In: Valley JW, Cole DR (eds) Stable Isotope Geochemistry, Reviews In Mineralogy and Geochemistry, vol 43, pp 365–414

Valley JW, Kitchen N, Kohn M, Niendorf CR, Spicuzza MJ (1995) UWG-2, a garnet standard for oxygen isotope ratios: strategies for high precision and accuracy with laser heating. Geochim Cosmochim Acta 59:5223–5231

Veizer J, Hoefs J (1976) The nature of O^{18}/O^{16} and C^{13}/C^{12} secular trends in sedimentary carbonate rocks. Geochim Cosmochim Acta 40:1387–1395

Weiblen PW, Morey GB (1980) A summary of the stratigraphy, petrology and structure of the Duluth Complex. Am J Sci 280:88–133

Zheng YF, Fu B (1998) Estimation of oxygen diffusivity from anion porosity in minerals. Geochem J 32:71–89